Journal of Applied Polymer Science

Breath Figure Templated Semifluorinated Block Copolymers with Tunable Surface Properties and Binding Capabilities

Lauri Valtola,[1] Mikko Karesoja,[1] Heikki Tenhu,[1] Petri Ihalainen,[2] Jawad Sarfraz,[2] Jouko Peltonen,[2] Melina Malinen,[3] Arto Urtti,[3] Sami Hietala[1]

[1]Laboratory of Polymer Chemistry, Department of Chemistry, University of Helsinki, Helsinki, Finland

[2]Department of Physical Chemistry, Åbo Akademi University, Porthansgatan 3-5 FIN-20500 Åbo, Finland

[3]Division of Biopharmaceutics and Pharmacokinetics, Faculty of Pharmacy, Centre for Drug Research, University of Helsinki, Helsinki, Finland

Correspondence to: S. Hietala (E-mail: sami.hietala@helsinki.fi)

ABSTRACT: Patterning of functionalized polymeric surfaces enables the adjustment of their characteristics and use in novel applications. We prepared breath figure (BF) films from three semifluorinated diblock copolymers, which all are composed of a polystyrene block and a semifluorinated one to compare their surface properties. "Click" chemistry was employed to one of the polymers, containing a poly(pentafluorostyrene) block to incorporate hydrophilic sugar or carboxylic acid moieties. The structure of the polymer alters the obtained porous morphology of the films. Contact angle (CA) analyses of the BF films reveals that the surface porosity increases water CAs compared with solvent cast films, and, in the case of hydrophobic polymers, leads to significant increase in the CAs of dodecane. The hydrophobicity of the BF films is further amplified by the removal of the topmost layer which leads in some cases to superhydrophobic surfaces. BF films containing glucose units are hydrophilic exhibiting water CAs below 90°. These glycosylated porous surfaces are shown to bind lectin Con A-FITC or can be labelled with isothiocyanate marker. © 2014 Wiley Periodicals, Inc. J. Appl. Polym. Sci. **2015**, *132*, 41225.

KEYWORDS: nanostructured polymers; porous materials; surfaces and interfaces

Received 8 May 2014; accepted 26 June 2014

DOI: 10.1002/app.41225

INTRODUCTION

Polymer surfaces with very high or low surface activity attract constant interest in the field of polymer science due to their wetting properties.[1,2] Films of semifluorinated polymers often exhibit low surface activity due to the surface enrichment of fluorinated units with inherent low surface activity leading to hydrophobicity and oleophobicity. If the roughness of such films is increased, superhydrophobic or superoleophobic surfaces can be realised. For example electrospinning of semifluorinated copolymers can lead to such superhydrophobic surfaces, even in the case where the fluorinated polymer is used only as a minor component in a blend with a homopolymer of the other block.[3] In electrospinning the polymers form fibres or particles that increase the roughness of the surface. However, the surface roughness can also be increased by introducing holes on the film surface. This can be done with various techniques including selective etching of components from self-assembled polymer film or by patterning with for example electron-beam lithography or (nano)imprinting.

"Breath figures" (BF)—structures made by condensing water vapor on a cold surface—have been studied since the early 20th century.[4–6] Many of the fundamental principles of the process, e.g., nucleation and kinetics of the formation of BFs on various surfaces are now relatively well understood.[7–9] BF templating using polymer solutions resulting in ordered polymeric films was first reported by Francois and coworkers[10,11] and has since been studied for various polymers and nanoparticles.[12–17] For making ordered solid polymeric films by BF technique a solution of polymer is typically deposited on a substrate in a humid environment so that evaporation of the volatile solvent induces water droplet condensation at the air/liquid interface. As the solvent continues to evaporate, the droplets grow and self-organize into an array. Under proper conditions the water droplets do not coalesce but instead, the concentrated polymer solution keeps them separated. When the solvent evaporates completely, the polymer forms a mold around the water droplets. When the water eventually evaporates it leaves arrays of pores in the polymer film, thereby also increasing the surface

Table I. Polymer Characteristics

Code	DP[a]	Mn_{NMR} (g/mol)	Mn_{SEC} (g/mol)	PDI
PS74	PS74		7800	1.1
PS-*b*-PFSF	PS89-*b*-PFSF4	11 900	11400	1.4
PS-*b*-PFMA	PS28-*b*-PFMA6	6100	3200	1.3
PS-*b*-PFS	PS74-*b*-PFS52	18000	27000	1.5

[a] Numbers denote degree of polymerization of the respective blocks based on SEC (PS homopolymer) or ^{1}H NMR.

roughness. When done appropriately, the pores can be ordered in a regular hexagonal pattern and their size can be controlled.

BF technique has been used to create regular porosity on various polymers using different solvents, surfaces or conditions. The pore size and pattern regularity are however dependent on numerous parameters. These include choice of solvent and polymer, polymer concentration, evaporation rate, and even the template.[12–15,18–20] Since the first reports[10] it has been observed that polymers that adopt a spherical shape are beneficial for the generation of regular porous structures.[13,14] Amphiphilic block copolymers in a selective solvent often form spherical aggregates and thus are a natural choice for BF formation. Use of block copolymers also allows the balancing of the hydrophilic and hydrophobic properties of the polymers that can be used to alter the morphology of the film.[13,14] In the case of semifluorinated polymers, it has been shown that[21,22] BF films of fluorinated polymers show decreasing pore size of films with increasing polymer fluorine content.

Such porous block copolymer films have various potential applications. The pores and their regular arrangement can be used to obtain for example separation materials, photoluminescence, biorecognition or cell adhesion as well as superhydrophobicity.[12–15,23,24] Superhydrophobicity or in general solvent repellency may be beneficial considering advanced anticorrosive coatings, surfaces with enhanced dirt repellency or in general for controlling wetting. Making use of amphiphilic polymers such as in the present case would have a beneficial effect in obtaining good adhesion with for example a conventional polymer coating due to the effect of the compatibilizing block. Further, with amphiphilic polymers there is a possibility to tailor the surface hydrophilicity or hydrophobicity by adjusting various chemical and templating parameters. This can lead to promotion or prevention of cell or biomolecule adhesion[25–27] or choice over either hydrophobic or hydrophilic segments are oriented toward the surface.[28,29] Due to the fact that the surface roughness of BF films can be easily modified by stripping the outer layer of the polymer film it enables an easy method to further adjust the surface wetting characteristics. Such treatment has earlier[30,31] resulted in needle-like surface with superhydrophobic and enhanced lipophobic properties of the surface after tape stripping.

In this report we focus on the use of semifluorinated block copolymers earlier used for making superhydrophobic electrospun surfaces[3] for generation and modification of honeycomb structured porous films. We show that the wetting properties of the BF films can be altered by the choice of polymer, manipulation of the surface structure or surface chemistry. Thus, the effects of the chemical composition of the polymer on the BF film formation and the resulting surface characteristics are the main focus of the present study. In addition, we compare the surface properties of the hydrophobic films to those prepared earlier with electrospinning[3] or solvent casting. By facile polymer modification we show that films made of these materials can be turned hydrophilic having different functional moieties on the surface, allowing their use in for example diagnostic or separation applications.

EXPERIMENTAL

Materials

The synthesis of the semifluorinated block copolymers, polystyrene-block-poly(perfluorooctyl ethyl methacrylate) (PS-*b*-PFMA), polystyrene-block-poly(2,3,5,6-tetrafluoro-4-(3,3,4,4,5,5,6,6,7,7,8,8,9,9,10,10,10-heptadecafluorodecaoxy)styrene) (PS-*b*-PFSF), polystyrene-block-polypentafluorostyrene (PS-*b*-PFS) has been published earlier.[3] The molecular characteristics of the polymers are shown in Table I. The reagents for PS-*b*-PFS modification, thioglycolic acid (Merck), 2,3,4,6-tetra-O-acetyl-1-thio-β-D-glucopyranose, SH-GlcAc4 (GLYCON Biochemicals GmBH), triethylamine (Fluka) as well as the analysis grade solvents (THF, chloroform, DMF, methanol) were used as received unless otherwise stated. The fluorescent markers, lectin-fluorescein isothiocyanate conjugate from Canavalia ensiformis (ConA-FITC) (Sigma-Aldrich), isothiocyanate Rhodamine B (RITC) (Sigma-Aldrich) and antifade reagent Prolong gold (Life Technologies) were used as received.

Modification of PS-*b*-PFS

The glucopyranose modification[32,33] of PS-*b*-PFS was done by dissolving PS-*b*-PFS (80 mg, 0.26 mmol repeating units of PFS) and SH-GlcAc4 (112.5 mg, 0.309 mmol) in 10 mL dry DMF followed by addition of triethyl amine (78 mg, 0.77 mmol) to the solution. After stirring for 4 h at room temperature, the reaction mixture was concentrated and precipitated into cold methanol. The white precipitate was filtered, washed twice with methanol, and dried in a vacuum oven to afford 158 mg of a white powder, PS-*b*-PFS-GlcAc4, (isolated yield 90%). The acetonide protected glycopolymer, PS-*b*-PFS-GlcAc4, was deprotected by adding sodium methanolate in methanol dropwise into PS-*b*-PFS-GlcAc4 (100 mg) dissolved in 10 mL of DMF and stirred for 1 h in room temperature. After stirring, the reaction mixture was concentrated and the deprotected PS-*b*-PFS-GlcOH precipitated into cold methanol. After drying in vacuum isolated yield of 63% was achieved. The thioglycolic acid substituted polymer, PS-*b*-PFS-COOH, was prepared by dissolving PS-*b*-PFS (80 mg, 0.26 mmol repeating units of PFS) and thioglycolic acid (29 mg, 0.309 mmol) in 10 mL dry DMF and triethyl amine (78 mg, 0.77 mmol) was added to the solution. After stirring for 4 h at room temperature, the reaction mixture was concentrated on a rotary evaporator to an approximate volume of 2.5 mL and precipitated into cold methanol. The white precipitate was filtered, washed twice with methanol, and dried in a vacuum oven to yield 83 mg of a white powder, PS-*b*-PFS-

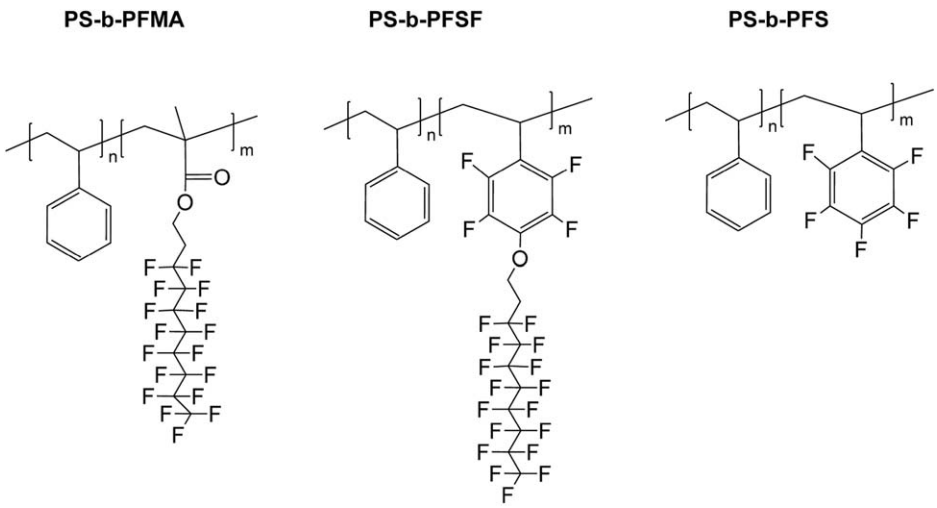

Scheme 1. Chemical structures of semifluorinated block copolymers.

COOH, (isolated yield) 80%. ^{1}H and ^{19}F NMR and IR were used to monitor the reactions.

Film Preparation via Breath Figure Templating

Polymers were dissolved in neat chloroform with polymer concentrations from 1 to 100 mg/mL. Piranha solution cleaned microscope glass slides were placed in humid environment (relative humidity 85%) and humid airflow was provided by bubbling air (2 mL/min) through a water vessel and directing the flow through an inverted funnel. Films were produced by injecting 5 μL of the polymer solution on the glass slides. For stripping the outermost polymer layer to expose the underlying structure an adhesive tape was firmly placed on the film and removed. As the deprotected PS-*b*-PFS-GlcOH polymer was poorly soluble in chloroform, glycopolymer films were made from PS-*b*-PFS-GlcAc4 followed by deprotection of the sugar residues on the film surface by immersing the BF films in methanol solution containing sodium methanolate for 2 h. The films were washed with deionized water and dried in air at room temperature. Prior to confocal fluorescence microscopy, the films were immersed either in aqueous rhodamine B isothiocyanate (RITC) solution (0.25 mg/mL) or FITC-conjugated concanavalin A (ConA-FITC) (0.2 mg/mL) in phosphate-buffered saline solution (PBS, 7.4) and incubated either for 3 or 6 h at room temperature, respectively. The labeled films were washed with deionized water several times, protected with Prolong gold antifade reagent, and covered with nro 0 cover glasses.

Characterization Methods

^{1}H and ^{19}F NMR measurements of the PS-*b*-PFS, PS-*b*-PFS-GlcAc4, PS-*b*-PFS-GlcOH, and PS-*b*-PFS-COOH were made with Bruker Avance III spectrometer operating at 500 MHz for protons. Scanning electron microscopy (SEM) experiments of the BF films were made with Hitachi S-4800 field emission scanning electron microscope from samples coated with Pt. Contact angle (CA) measurements were conducted with a KSV CAM 200 instrument using distilled water (CA_{water}) or dodecane (CA_{dodec}). IR measurements were carried out with Bruker Alpha ATR-FTIR instrument.

Atomic force microscopy (AFM) was carried out with a NTEGRA Prima atomic force microscope. Topographical imaging was carried out by an intermittent-contact mode under ambient conditions using silicon cantilevers with a nominal tip radius of 10 nm (Model NSG10). The images (1024 $\times$ 1024 pixels) were recorded in the repulsive regime using a damping ratio of 0.6 and a scan speed of 0.25 Hz. The images were analyzed with the Scanning Probe Image Processor software.

The X-ray photoelectron spectroscopy (XPS) spectra were obtained with a PHI Quantum 2000 scanning spectrometer, using monochromatic Al Kα (1486.6 eV) excitation and charge neutralization by using an electron filament and an electron gun. The photoelectrons were collected at 45° in relation to the sample surface with a hemispherical analyser. The analyzing depth was approximately 5–10 nm. The pass energy was 187.85eV and the acquisition time was 10–12 min. The measurements were carried out on at least three different spots for each sample.

The interaction of fluorescent probes with the films was examined using a Leica TCS SP5 confocal laser scanning system with Leica DM5000 upright microscope, HCX APO 63x/1.30 Corr (glycerol) CS 21 objective and DD 488/561 beam splitter. RITC stained samples were excited with 561 nm at 20 mW and emission was collected at 568–617 nm. The films treated with ConA-FITC were excited with 488 nm at 270 mW and emission was recorded at 500–550 nm. Fluorescence images were taken at different depths with an axial depth resolution of 0.25 μm and additionally transmitted light was recorded. Slice images were constructed with Imaris 7.6 software (Bitplane) without deconvolution.

RESULTS AND DISCUSSION

The chemical structures of the semifluorinated diblock copolymers and modified PS-*b*-PFS are outlined in Schemes 1 and 2 and the polymer characteristics are given in Table I. The modification of the pentafluorostyrene units of PS-*b*-PFS was performed with two thiols, thioglycolic acid and 2,3,4,6-tetra-O-acetyl-1-thio-β-D-glucopyranose (SH-GlcAc4), shown in

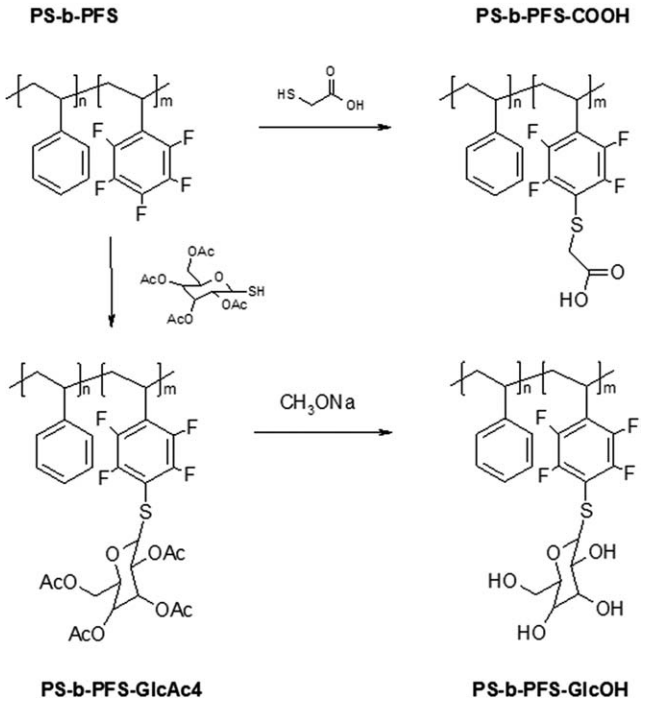

Scheme 2. Modification of the PS-*b*-PFS with thiols.

Scheme 2. ^{1}H NMR spectra, Figure 1, show the appearance of both the acetylated glucose units as well as the CH_2 protons of the thioglycolic acid. ^{19}F NMR spectra of both substituted polymers confirm the partial substitution of the *para*-fluorine position in pentafluorostyrene units, 90% in the case of PS-*b*-PFS-GlcAc4 and 14 % in the case of PS-*b*-PFS-COOH, see Figure 2. The deprotection of the acetyl groups of PS-*b*-PFS-GlcAc4 was monitored by ^{1}H NMR, the spectra showing the disappearance of acetyl groups in the spectra of PS-*b*-PFS-GlcOH at 2 ppm as shown in Figure 1.

Breath Figure Formation of PS-*b*-PFS, PS-*b*-PFSF, and PS-*b*-PFMA

The copolymers dissolve readily in chloroform up to the studied polymer concentration of 100 mg/mL, forming clear solutions.

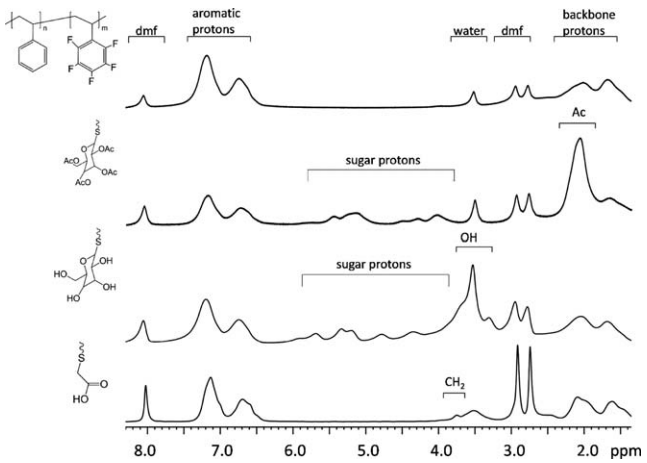

Figure 1. ^{1}H NMR (DMF-d7) spectra of PS-*b*-PFS, PS-*b*-PFS-GlcAc4, PS-*b*-PFS-GlcOH, and PS-*b*-PFS-COOH.

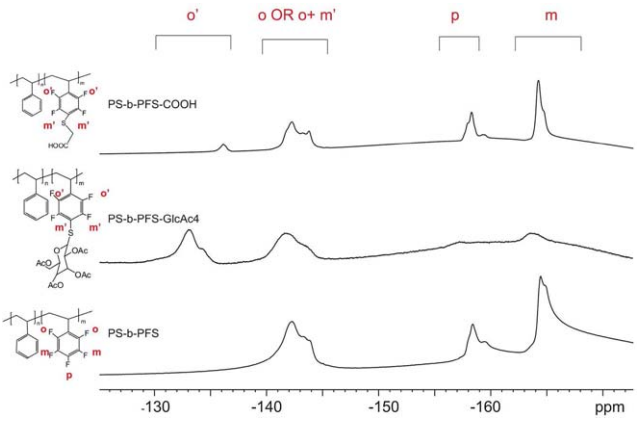

Figure 2. ^{19}F NMR spectra (DMF-d7) of PS-*b*-PFS, PS-*b*-PFS-GlcAc4, and PS-*b*-PFS-COOH. [Color figure can be viewed in the online issue, which is available at wileyonlinelibrary.com.]

In breath-figure templating, the parameters controlling the formation of pores are numerous and include for example the choice of solvent, air flow rate, humidity, additives, interfacial activity of polymers, as well as the concentration and amount of the polymer solution.[13] In the present case the effect of polymer concentration was studied. The SEM analyses of the BF films made with different polymer concentrations revealed that below the polymer concentration of 50 mg/mL regular BFs were obtained on rather small areas accompanied with large disordered or flat areas (data not shown). When the polymer concentration was 50 or 100 mg/mL, large areas containing pores were formed, see Figure 3 and Table II. For the hydrophobic semifluorinated films higher polymer concentration, 100 mg/mL, gave smaller pores compared with 50 mg/mL and at the same time the pore size distribution became narrower. It is evident that increased polymer concentration stops the growth of the water droplets at an earlier stage and leads to the formation of smaller pores. These findings are in agreement with previous reports,[5] where the pore size has been found to be inversely concentration dependent and the size distribution has also narrowed with polymer concentration. The sizes of the pores for different hydrophobic polymers varied from 0.43 to 1.26 μm depending on the polymer and concentration. The reasons for the variation are related to the differences in surface activity and molar mass of the polymers which alter the nucleation of water droplets. It has earlier been reported for polyethylene oxide-poly(perfluoro octyl methacrylate) diblock polymers that the pore size increased with increasing length of the fluorinated block.[17] This was concluded to reflect the increased water droplet nucleation rate for shorter fluorinated blocks and correlates with our results. Studies on linear poly(*tert*-butyl acrylate-*block*-poly(2-[(perfluorononenyl)oxy]ethyl methacrylate)[21] and star-like poly[(*1H,1H*-pentafluoropropyl acrylate)-*ran*-(methyl methacrylate)][22] polymers on the other hand have shown that the average pore diameter decreases with greater fluorinated monomer content. This is attributed to the increasing hydrophobicity accelerating the polymer aggregation/precipitation rate at the solution/water interface during casting. In the present case, the PS-*b*-PFSF and PS-*b*-PFMA polymers have very high surface activity due to the fluorinated methyl groups compared with

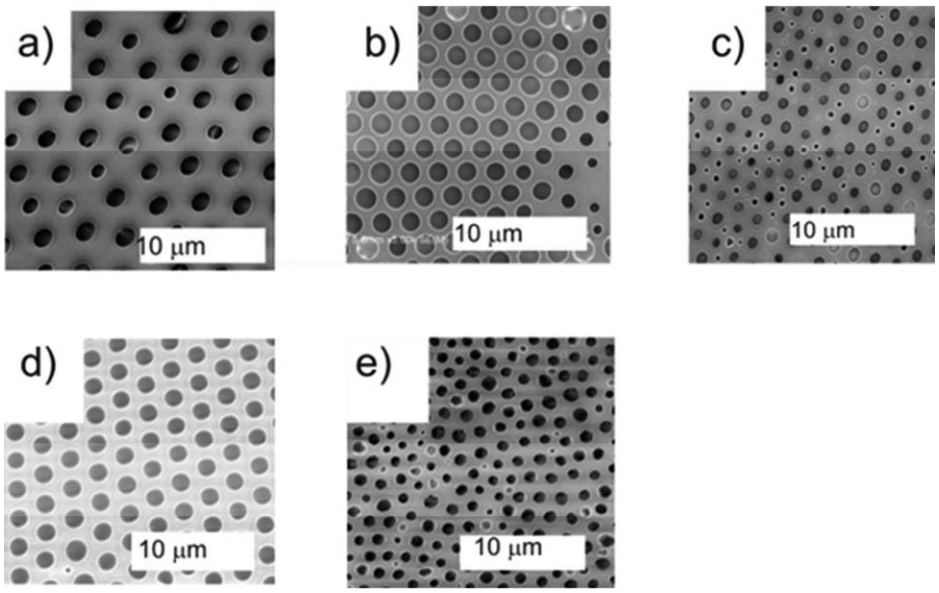

Figure 3. Scanning electron micrographs of breath figure films of PS-*b*-PFS (a), PS-*b*-PFMA (b), PS-*b*-PFSF (c), PS-*b*-PFS-GlcAc4 (d), and PS-*b*-PFS-COOH (e). Polymer concentrations 50 mg/mL in $CHCl_3$.

the PS-*b*-PFS regardless of their shorter fluorinated block length.[3] Thus the smaller pore size for PS-*b*-PFSF and PS-*b*-PFMA polymers originates both from the shorter fluorinated block lengths and their larger surface activity.

A cross-section SEM image of the PS-b-PFS, Figure 4, reveals that under the present conditions the pores do not extend to the bottom of the film, but instead are formed by condensation of water droplets in the top layer, leaving a solid non-porous polymer film beneath the porous structure. The depth of the pores in the case of PS-b-PFS is roughly 1.7 μm and the diameter of the underlying pores is $\sim$3 μm compared with average pore diameter of 1.26 μm observed on the surface. It is also clearly seen that the porous surface layer is supported with pillar-like structures forming the pore walls.

Surface Modification by Tape Peeling

In order to reveal the structure below the surface pores an adhesive tape was applied to the film surface and the top layer was peeled by detaching the tape from the surface.[30] SEM images of the interface between porous nondamaged surface and of the fractured surface after peeling are shown in Figure 5. As already shown in the cross-section SEM image in Figure 4, the pore diameters beneath the surface are larger than that observed on the surface. Although some of the pillar structures between the surface holes might be destroyed by the peeling process, the SEM images of the peeled film indicate that some of the pores on the surface may originate from interconnected pores or that some of the surface pores have merged during the drying process, especially in the case of PS-*b*-PFS.

Thioglycolic Acid and Glucopyranose-Modified BF Films

PS-*b*-PFS-GlcAc4 and PS-*b*-PFS-COOH also form honeycomb structures as shown in Figures. 3 and 6. The deprotected glycopolymer, PS-*b*-PFS-GlcOH, does not fully dissolve in chloroform and the resulting BF films consisted of aggregates instead of porous structures (data not shown). Therefore the glycosylated BF films were prepared with acetylated polymer and then, the sugar moieties were deprotected on the surface. The surface deprotection did not significantly alter the pore structure as can be seen from Table II and comparison of Figures 3(d) and 6(b). IR measurements, Figure 7, confirm that the carboxyl peaks of the acetal groups disappear upon the surface treatment. XPS analyses of these BF films confirm the presence of sulphur close to the surface (5–10 nm). While no sulphur is detected in the PS-*b*-PFS, the fluorine to sulphur ratio was found to be 118 for PS-*b*-PFS-COOH and 6 for the PS-*b*-PFS-GlcAc4, corresponding well to the analysis of the substitution degree of thioglycolic acid and glucopyranose units with NMR.

Somewhat surprisingly, the increase of polymer concentration from 50 to 100 mg/mL leads to increased pore size for the PS-*b*-

Table II. Average Pore Sizes from SEM and AFM Analysis from Films with Different Casting Conditions

	Average pore size/μm				
Polymer concentration	PS-*b*-PFSF	PS-*b*-PFMA	PS-*b*-PFS	PS-*b*-PFS-GlcAc4	PS-*b*-PFS-COOH
$CHCl_3$ 50 mg/mL	0.72	1.34	1.26/1.45[a]	1.34/1.20[b]	0.84
$CHCl_3$ 100 mg/mL	0.67	0.43	0.63	1.58	1.00

[a] Value from AFM analysis.
[b] Value from AFM analysis of PS-*b*-PFS-GlcOH.

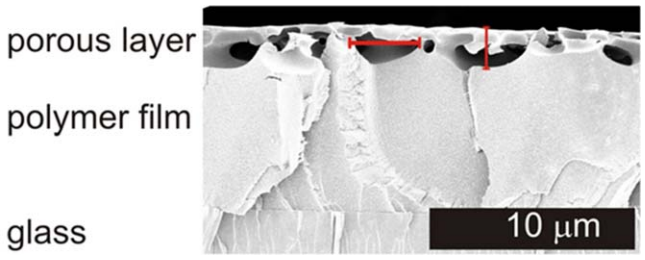

Figure 4. Cross-section SEM image of PS-*b*-PFS BF film with scale bars indicating the depth and diameter of the pores. Polymer concentration 50 mg/mL in $CHCl_3$. [Color figure can be viewed in the online issue, which is available at wileyonlinelibrary.com.]

PFS-COOH and PS-*b*-PFS-GlcAc4 BF films, Table II. This contradicts with the suggested scaling relation[13] where an increase in polymer concentration should lead to a decreased pore size. The unmodified hydrophobic fluorinated polymers in the present case were indeed found to follow this rule, but it appears that when the amphiphilic polymers contain a hydrophilic block as in the case of PS-*b*-PFS-GlcAc4 and PS-*b*-PFS-COOH, the pore size may decrease with increasing concentration. It has earlier been observed for BF films made from triblock dendritic poly (L-lysine)-*b*-poly(L-lactide)-*b*-dendritic poly(L-lysine) polymers[34] that pore sizes increased when the polymer concentration in chloroform was increased from 0.1 to 0.8 w/v. In the case of linear-dendritic polymers comprising of polyethylene glycol (PEG)-polycaprolactone (PCL) polymers (PEG2k-G3-PLA30),[35] where the PCL blocks are linked to 3rd generation *bis*-methylpropionic acid (bis-MPA) dendrons, a size increase was also observed for when polymer concentration in benzene was increased from 1 to 2.5 mg/mL. The reason for the pore size increase with increasing polymer concentration in the abovementioned and in the present case may be explained by the the strong interaction of the water with the hydrophilic part, which leads to slowing down of the evaporation of the volatile solvent. The evaporation rate may also be slowed down due to increased solution viscosity. Correspondingly, this leads to a decrease in the temperature difference, thus increasing the water-droplet growth time.[34,36] The final size of the water droplets are both dependent on the temperature difference and the water-droplet growth time. When the droplet growth time becomes the major factor, it results in larger size droplets by uptake of moisture. It appears that in the present case with polymers with hydrophilic blocks this effect overcomes the usually observed pore size decrease of hydrophobic amphiphiles.

The SEM and AFM analysis of the PS-*b*-PFS-GlcAc4 and PS-*b*-PFS-GlcOH BF films show that the pores are larger than for the PS-*b*-PFS-COOH BF films. Due to the smaller degree of substitution in the case of PS-*b*-PFS-COOH is less hydrophilic than the PS-*b*-PFS-GlcAc4 explaining the smaller pore size.

Surface Wetting Properties

In many cases the fluorinated groups in semifluorinated copolymers have a tendency to phase separate and enrich on the surface leading to increased hydrophobicity and oleophobicity of the films. Especially the fluoromethyl, CF_3, groups are effective, resulting in many cases in superhydrophobic or very oleophobic

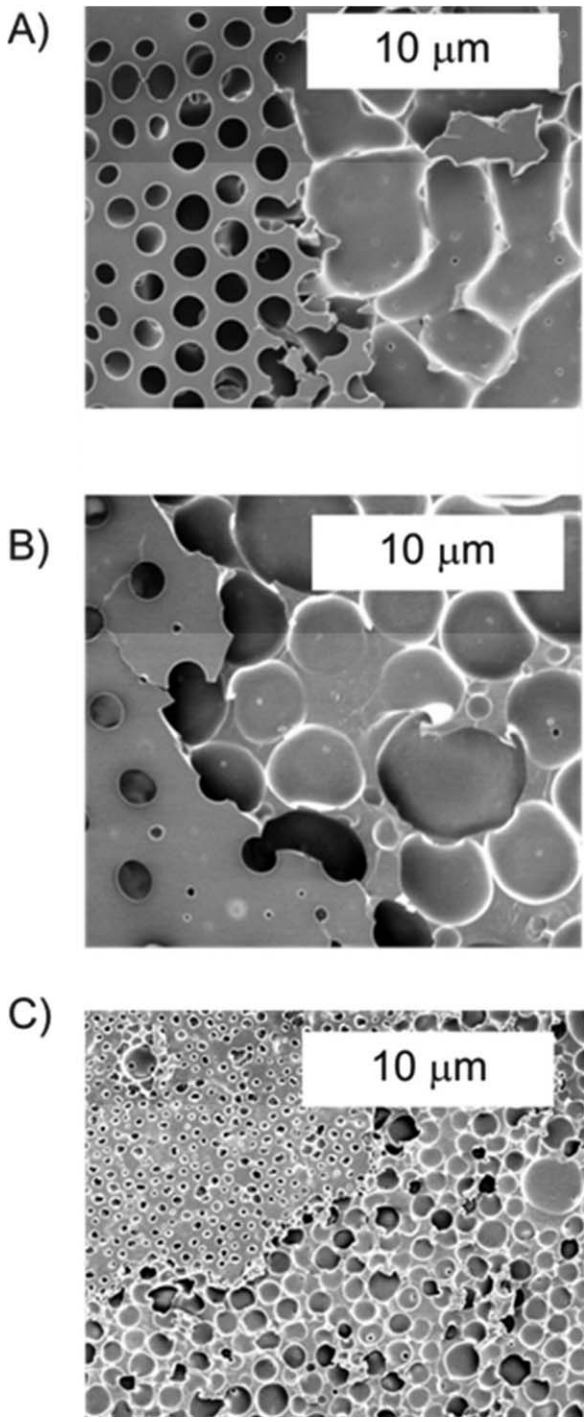

Figure 5. SEM images of the tape stripped interface of honeycomb structured films of (A) PS-*b*-PFS (B) PS-*b*-PFMA, and (C) PS-*b*-PFSF. Polymer concentrations 50 mg/mL in $CHCl_3$.

surface. When the polymers were electrospun as micrometer sized particles or fibrous mats, they showed increased hydrophobicity compared with flat solvent casted films, or even superhydrophobicity when fluoromethyl group containing polymers were used.[3] In the electrospinning process the particles or fibres solidify quickly under rather dry conditions, leading to enrichment of the fluorinated units on their surface, thereby enhancing their hydrophobicity. On the other hand, in the BF

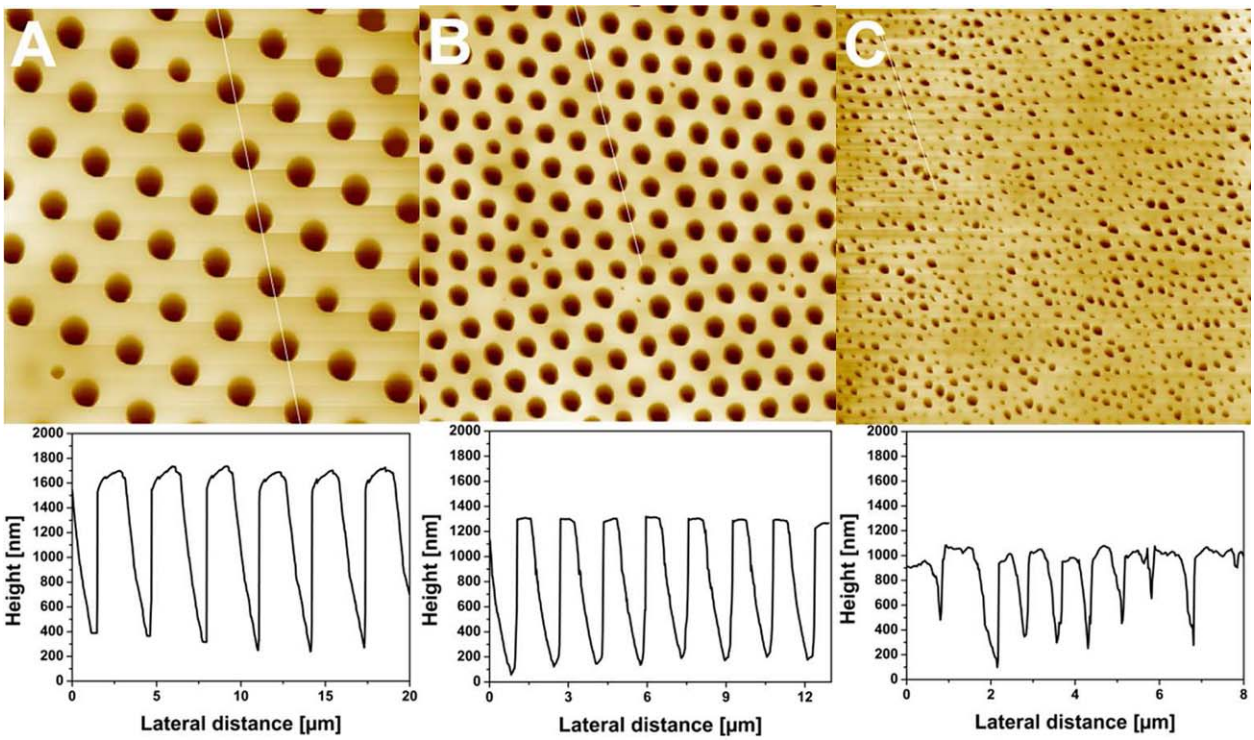

Figure 6. AFM topographs (image size 20 × 20 μm) of (A) PS-*b*-PFS (height scale 2 μm), (B) PS-*b*-PFS-GlcOH (height scale 1.5 μm), and (C) PS-*b*-PFS-COOH (height scale 1.2 μm). Also shown are line profiles for respective samples over the porous structure. [Color figure can be viewed in the online issue, which is available at wileyonlinelibrary.com.]

technique water is usually used as the templating solvent and therefore could cancel the enrichment of fluorinated moieties on the surface. To examine the effect of the BF process on the surface properties of the block copolymers, CAs of water (CA_{water}) and dodecane (CA_{dodec}) were compared between flat surfaces made by solvent casting, BF films and tape stripped BF films. As shown in Table III, the BF films without thioglycolic acid or glucose in general exhibit higher CAs compared with solvent casted films and, more importantly, the fluoromethyl containing polymers have highest CAs for both water and dodecane. Thus it appears that the presence of water in the BF process does not significantly alter the enrichment of fluorinated moieties on the surface. The roughness of the surface also plays an important role in wetting and the increased surface roughness of the porous BF films compared with flat solvent casted ones explains the increased CAs. However, compared with the electrospun materials, the BF films are less hydrophobic due to their smaller roughness.

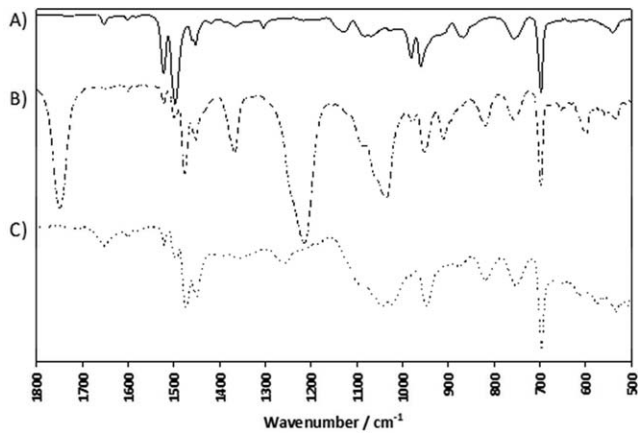

Figure 7. IR spectra of BF films of PS-*b*-PFS (A), PS-*b*-PFS-GlcAc4 (B), and PS-*b*-PFS-GlcOH (C).

When BF films with different pore sizes are compared, it is evident that the chemical nature of the film is the main factor. Comparing the PS-*b*-PFS made with 50 mg/mL (average pore size 1.26 μm) to the PS-*b*-PFMA (1.43 μm) and PS-*b*-PFSF (0.72 μm), both CF_3 containing polymers have much more pronounced hydro- and oleophobicity. On the other hand, PS-*b*-PFS BF films made from 50 or 100 mg/mL chloroform solutions have similar water CAs indicating that the difference in pore sizes at this size range does not alter the CA. For the BF films the surface roughness can be increased by tape stripping the uppermost film surface. As shown in Table III, these peeled BF film surfaces show significantly increased CA_{water} compared with either flat films or unmodified BF films. The polymers having CF_3 groups, PS-*b*-PFMA and PS-*b*-PFSF, somewhat surprisingly show smaller increase in CA_{water} compared to PS-*b*-PFS. Here the different pillar structure of the peeled films explains the difference. As shown in Figures 4 and 5, the underlying pore structure of PS-*b*-PFS consists of much larger pores and the increase in surface roughness is larger than in the case of the two other films. Consequently, the CA_{water} increases due to the increased roughness and the peeled PS-*b*-

Table III. Contact Angles of Different Films. Data for BF Films Made with 50 mg/mL Polymer Concentration in $CHCl_3$

	Solvent casted films		Breath figure films	
Sample	CA water/°	CA dodecane/°	CA water/°	CA dodecane/°
PS-*b*-PFSF	111	73	116	72
PS-*b*-PFSF peeled	-	-	130	45
PS-*b*-PFMA	116	68	118	85
PS-*b*-PFMA peeled	-	-	153	93
PS-*b*-PFS	96	52	112	30
PS-*b*-PFS peeled	-	-	155	18
PS-*b*-PFS-COOH	93	7	106	47
PS-*b*-PFS-GlcAc4	75	<5	100	10
PS-*b*-PFS-GlcOH	70	<5	89	-

PFMA and PS-*b*-PFS films are superhydrophobic (CA_{water} >150°). The CA_{dodec} is similarly affected by the chemical nature of the films, the CF3 containing polymers having the highest CA_{dodec}. However, for most of the peeled surfaces CA_{dodec} decreases compared with the BF films, which is due to the low surface tension of dodecane that allows it to spread on the rough peeled surfaces.

For the glucopyranose or thioglycolic acid containing polymers the CA_{water} and CA_{dodec} are significantly lower compared with the PS-*b*-PFS. For the deprotected glucose-modified film, PS-*b*-PFS-GlcOH, the surface becomes hydrophilic (CA_{water} <90°) both for a flat solvent casted film and the BF film. The switching of the surface from hydrophobic to hydrophilic is beneficial when considering possible applications in detection of water-soluble biomarkers, because the analytes can more efficiently wet the pores beneath the surface.

Biorecognition Utilizing the BF Films

Molecular recognition experiments were carried out to study the ligand binding capability of the glucose containing PS-*b*-PFS-GlcOH BF films. Two sugar-binding fluorescent markers, lectin ConA-FITC and Rhodamine B isothiocyanate (RITC) were used to study the interaction with the films. PS-*b*-PFS and PS-*b*-PFS-COOH BF films were used as a control. The cross section fluorescence images taken at 1 μm depth from the surface are shown in Figure 5. As the fluorescence signal arises specifically from the selected focal plane it can reveal specifically where the marker is bound.

The PS-*b*-PFS BF films, Figure 8(a,c), incubated with the fluorescent markers show only weak fluorescence signals regardless of the scanning depth. The hydrophilic control sample, PS-*b*-PFS-COOH, behaves similarly. Both samples thus show that the marker is effectively removed during the washing step, apart from maybe a small amount of marker trapped in the pores. On the other hand, the BF film of PS-*b*-PFS-GlcOH, Figure 8(b), shows that Con A-FITC gives intense fluorescence signal mainly from the pore walls at the selected depth focus. Deeper scanning depth showed that also the bottom of PS-*b*-PFS-GlcOH is covered with the fluorescence marker. The other studied fluorescence marker, RITC, is able to bind to glucose moieties via the reaction of isothiocyanate groups. Again for the PS-*b*-PFS-GlcOH intense fluorescence inside the pores can be seen as shown in Figure 8(d). These results indicate that the glucose bearing BF films have capability of binding the fluorescent markers both via specific protein-sugar interactions in the case of Con A and via chemical reactions in the case of rhodamine B.

This work demonstrates that BF processing of semifluorinated block copolymers can be used in creating a versatile platform for bioanalytics and other applications that benefit from the porosity and/or tunability of surface properties. The ease of post-modifying the pentafluorostyrene units multiplies the number of

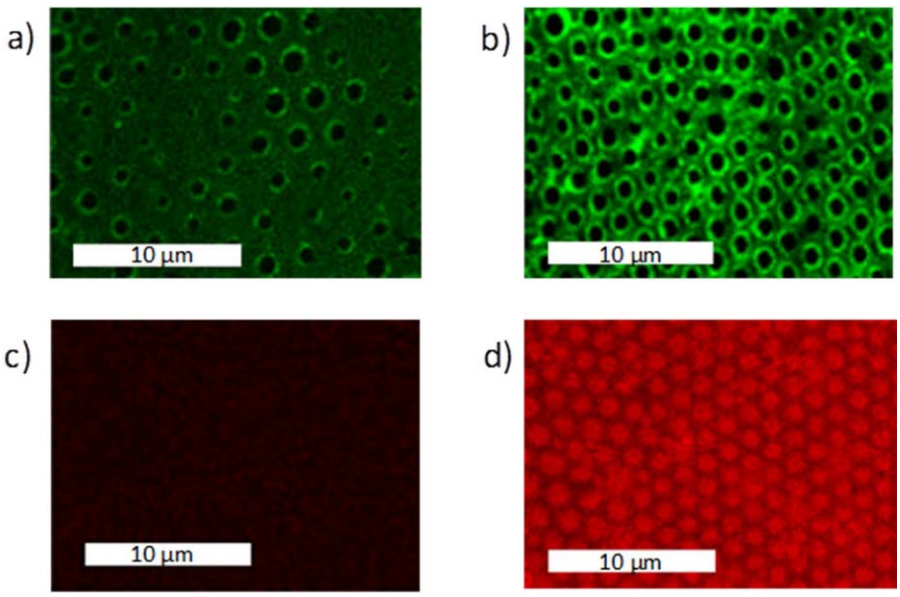

Figure 8. Cross section images of confocal microscopy obtained from the films stained with Con A-FITC (a) PS-*b*-PFS, (b) PS-*b*-PFS-GlcOH and RITC (c) PS-*b*-PFS, (d) PS-*b*-PFS-GlcOH. [Color figure can be viewed in the online issue, which is available at wileyonlinelibrary.com.]

accessible polymer derivatives. A vast library of thiolated substances may be used and the degree of substitution can be adjusted. The chemistry combined with the mechanical manipulation of the surface could lead to miniaturized, biorecognizing surfaces.

CONCLUSIONS

Semifluorinated diblock copolymers based on polystyrene (PS) as the other block and polypentafluorostyrene (PFS), poly (perfluorooctyl ethyl methacrylate) (PFMA) or poly(2,3,5,6-tetrafluoro-4-(3,3,4,4,5,5,6,6,7,7,8,8,9,9,10,10,10-heptadecafluorodecaoxy)styrene) (PFSF) as the other block were casted as honeycomb structured films utilizing BF templating technique. The films were obtained using chloroform as the solvent and the pore sizes varied from 0.2 to 1.7 μm depending on the polymer used and the polymer concentration. For the polymers containing only hydrophobic blocks increasing polymer concentration lead to smaller sized pores. The surfaces of the porous films of PS-*b*-PFS, PS-*b*-PFMA, and PS-*b*-PFSF were more hydro- and oleophobic than flat solvent casted films due to the increased roughness. Peeling off the top layer further increased the roughness and the hydrophobicity increased, leading to superhydrophobic surfaces in case of PS-*b*-PFS and PS-*b*-PFMA. The pentafluorostyrene units of the PS-*b*-PFS were further modified with thioglycolic acid or a thiolated glucopyranose. For these polymers containing a hydrophilic block increase in polymer concentration in the casting solvent increased the sizes of the pores. The water CAs decreased with the introduction of hydrophilic units and for the glucose-modified BF film, PS-*b*-PFS-GlcOH, the surface turned hydrophilic with water CA $<90°$. Finally, fluorescence microscopy showed that the pores of the glucose containing BF films bind fluorescent markers lectin Con A-FITC via specific protein–sugar interactions and rhodamine B isothiocyanate by a chemical reaction between the glucose units and isothiocyanate.

ACKNOWLEDGMENT

Financial support is acknowledged from the Academy of Finland through the FUNMAT Center of Excellence for Functional Materials.

REFERENCES

1. Shirtcliffe, N. J.; McHale, G. I. Newton, M. *J. Polym. Sci. Part B: Polym. Physics* **2011**, *49*, 1203.
2. Stratakis, E.; Mateescu, A.; Barberoglou, M.; Vamvakaki, M.; Fotakis, C.; Anastasiadis, S. H. *Chem. Commun.* **2010**, *46*, 4136.
3. Valtola, L.; Koponen, A.; Karesoja, M.; Hietala, S.; Laukkanen, A.; Tenhu, H.; Denifl, P. *Polymer* **2009**, *50*, 3103.
4. Rayleigh, L. *Nature* **1911**, *86*, 416.
5. Aitken, J. *Nature* **1911**, *86*, 516.
6. Rayleigh, L. *Nature* **1912**, *90*, 436.
7. Beysens, D.; Knobler, C. M. *Phys. Rev. Lett.* **1986**, *57*, 1433,
8. Fritter, D.; Beysens, D.; Knobler, C. M. *Phys. Rev. A.* **1991**, *43*, 2858.
9. Steyer, A.; Guenoun, P.; Beysens, D.; Knobler, C. M. *Phys. Rev. A.* **1991**, *44*, 8271.
10. Widawski, G.; Rawiso, M.; François, B. *Nature* **1994**, *369*, 387.
11. François, B.; Pitois, O.; François, J. *Adv. Mater.* **2004**, *7*, 1041.
12. Bunz, U. H. F. *Adv. Mater.* **2006**, *18*, 973.
13. Hernandez-Guerrero, M.; Stenzel, M. H. *Polym. Chem.* **2012**, *3*, 563.
14. Escalé, P.; Rubatat, L.; Billon, L.; Save, M. *Eur. Polym. J.* **2012**, *48*, 1001.
15. Muñoz-Bonilla, A.; Fernández-García, M.; Rodríguez-Hernández, J. *Prog. Polym. Sci.* **2014**, *39*, 510.
16. Srinivasarao, M.; Collings, D.; Philips, A.; Patel, S. *Science* **2001**, *292*, 79.
17. Saunders, A. E.; Dickson, J. L.; Shah, P. S.; Lee, M. Y.; Lim, K. T.; Johnston, K. P.; Korgel, B. A. *Phys. Rev. E* **2006**, *73*, 031608.
18. Ferrari, E.; Fabbri, P.; Pilati, F. *Langmuir* **2011**, *27*, 1874.
19. Cui, L.; Peng, J.; Ding, Y.; Li, X.; Han, Y. *Polymer* **2005**, *46*, 5334.
20. Peng, J.; Han, Y.; Yang, Y.; Li, B. *Polymer* **2004**, *45*, 447.
21. Qin, S.; Li, H.; Yuan, W.; Zhang, Y. *J. Mater. Sci.* **2012**, *47*, 6862.
22. Zhang, Z.; Hughes, T. C.; Gurr, P. A.; Blencowe, A.; Uddin, H.; Hao, X.; Qiao, G. G. *Polymer* **2013**, *54*, 4446.
23. Wan, L.-S.; Li, J.-W.; Ke, B.-B.; Xu, Z.-K. *J. Am. Chem. Soc.* **2012**, *134*, 95.
24. Wan, L.-S.; Zhu, L.-W.; Ou, Y.; Xu, Z.-K. *Chem. Commun.* **2014**, *50*, 4024.
25. Hernández-Guerrero, M.; Min, E.; Barner-Kowollik, C.; Müller, A. H. E.; Stenzel, M. H. *J. Mater. Chem.* **2008**, *18*, 4718.
26. Beattie, D.; Wong, K. H.; Williams, C.; Poole-Warren, L. A.; Davis, T. P.; Barner-Kowollik, C.; Stenzel, M. H. *Biomacromolecules* **2006**, *7*, 1072.
27. Wu, X.; Wang, S. *ACS Appl. Mater. Interfaces* **2012**, *4*, 4966.
28. Muñoz-Bonilla, A.; Ibarboure, E.; Papon, E.; Rodriguez-Hernandez, J. *Langmuir* **2009**, *25*, 6493.
29. Muñoz-Bonilla, A.; Ibarboure, E.; Papon, E.; Rodriguez-Hernandez, J. *J. Polym. Sci. Part A: Polym. Chem.* **2009**, *47*, 2262.
30. Yabu, H.; Takebayashi, M.; Tanaka, M.; Shimomura, M. *Langmuir* **2005**, *21*, 3235.
31. Kim, J.; Lew, B.; Kim, W. S. *Nanoscale Res. Lett.* **2011**, *6*, 616.
32. Becer, C. R.; Babiuch, K.; Pilz, D.; Hornig, S.; Heinze, T.; Gottschaldt, M.; Schubert, U. S. *Macromolecules* **2009**, *42*, 2387.
33. Riedel, M.; Stadermann, J.; Komber, H.; Simon, F.; Voit, B. *Eur. Polym. J.* **2011**, *47*, 675.
34. Zhu, Y.; Sheng, R.; Luo, T.; Li, H.; Sun, J.; Chen, S.; Sun, W.; Cao, A. *ACS Appl. Mater. Interfaces* **2011**, *3*, 2487.
35. Walter, M. V.; Lundberg, P.; Hult, D.; Hult, A.; Malkoch, M. *Polym. Chem.* **2013**, *4*, 2680.
36. Pitois, O.; Francois, B. *Colloid Polym. Sci.* **1999**, *277*, 574.